Available online at www.sciencedirect.com
SCIENCE DIRECT®
Journal of Magnetic Resonance 167 (2004) 298–305
JMR Journal of Magnetic Resonance
www.elsevier.com/locate/jmr

Time resolved spectroscopic NMR imaging using hyperpolarized ^{129}Xe

S. Han,[a] H. Kühn,[b] F.W. Häsing,[c] K. Münnemann,[b] B. Blümich,[b] and S. Appelt[c,*]

[a] *Max-Planck Institute for Polymer Research, Ackermannweg 10, D-55128, Mainz, Germany*
[b] *Institute of Macromolecular Chemistry and Technical Chemistry, RWTH-Aachen, D-52056, Germany*
[c] *Zentrallabor für Elektronik, Forschungszentrum Jülich, D-52425, Jülich, Germany*

Received 18 September 2003; revised 19 December 2003

Abstract

We have visualized the melting and dissolution processes of xenon (Xe) ice into different solvents using the methods of nuclear magnetic resonance (NMR) spectroscopy, imaging, and time resolved spectroscopic imaging by means of hyperpolarized ^{129}Xe. Starting from the initial condition of a hyperpolarized solid Xe layer frozen on top of an ethanol (ethanol/water) ice block we measured the Xe phase transitions as a function of time and temperature. In the pure ethanol sample, pieces of Xe ice first fall through the viscous ethanol to the bottom of the sample tube and then form a thin layer of liquid Xe/ethanol. The xenon atoms are trapped in this liquid layer up to room temperature and keep their magnetization over a time period of 11 min. In the ethanol/water mixture (80 vol%/20%), most of the polarized Xe liquid first stays on top of the ethanol/water ice block and then starts to penetrate into the pores and cracks of the ethanol/water ice block. In the final stage, nearly all the Xe polarization is in the gas phase above the liquid and trapped inside the pores. NMR spectra of homogeneous samples of pure ethanol containing thermally polarized Xe and the spectroscopic images of the melting process show that very high concentrations of hyperpolarized Xe (about half of the density of liquid Xe) can be stored or delivered in pure ethanol.

Keywords: NMR spectroscopy; Magnetic resonance imaging; Hyperpolarized xenon; Materials science

1. Introduction

Nuclear magnetic resonance (NMR) of Xe is known as a very sensitive method for monitoring chemical and structural environments. Due to the low signal-to-noise ratio of NMR from Xe in thermodynamic equilibrium, the acquisition of a single NMR spectrum in materials is usually very time consuming, taking 10 min up to tens of hours. NMR with hyperpolarized Xe has overcome this problem and therefore the number of applications in material sciences and medicine has increased significantly in the recent years [1–8]. The large nuclear magnetization of hyperpolarized Xe allows the repetitive application of excitation pulses with very small flip angles, slowly consuming the non-equilibrium magnetization and therefore eliminating the need of T_1-waiting periods between successive measurements. This makes time resolved Xe spectroscopy and imaging viable.

A series of hyperpolarized Xe spectra supply information about structural and chemical changes evolving in time. Many experiments have been demonstrated using time resolved NMR spectroscopy with hyperpolarized Xe, such as the diffusion of Xe into porous glass [9], the xenon exchange between two phases in soft porous materials [10], and the formation of clathrate structures [11–14]. Xenon magnetic resonance imaging (MRI) and flow imaging measure the distribution of the Xe spin density and the motional information as a function of space, and do not provide information about the structural or chemical environment. Tseng et al. [15] demonstrated MRI of laser polarized liquid Xe with high resolution and Mair et al. [16] investigated the spin density, diffusion, and velocity distribution of a stationary convection pattern of hyperpolarized Xe.

* Corresponding author. Fax: +49-2461-613-990.
E-mail address: st.appelt@fz-juelich.de (S. Appelt).

1090-7807/$ - see front matter © 2004 Elsevier Inc. All rights reserved.
doi:10.1016/j.jmr.2004.01.004

Xenon spectroscopic imaging, also known as chemical shift imaging (CSI), is able to measure both, chemical and spin density properties of a sample but normally at the cost of a much longer measuring time because an additional dimension is added. A first 2D CSI image with hyperpolarized Xe was done by Swanson et al. [2] in a rat brain. Moudrakovski et al. [17] showed that with a stationary continuous flow of hyperpolarized Xe the time required for acquisition of a 2D spectroscopically resolved image is reduced from tens of hours to about 30 min. However, if Xe spectroscopic imaging is used for characterizing dynamic processes varying on a timescale of seconds, a complete image must be acquired in less than one second. We demonstrate that this is possible if a large reservoir of hyperpolarized Xe with a high polarization fraction (~20%) is provided [18] and only one spatial dimension is chosen beside the spectroscopic dimension (1D CSI).

An important issue is the storage of large quantities of hyperpolarized Xe in solids and liquids. Furthermore, the delivery of high concentrations of hyperpolarized Xe to macro- or biomolecules in aqueous and non-polar solvents is essential for the investigation of the structure of these molecules using Xe and/or SPINOE NMR [3,4,18]. For this purpose, the solvent ethanol is promising because it can be mixed with water in arbitrary proportions. Therefore, we have investigated the dynamics of melting, migration, and dissolution of hyperpolarized Xe ice into ethanol and ethanol/water mixtures with the method of time resolved spectroscopic imaging.

2. Experimental

We produce the hyperpolarized Xe using a continuous flow Rb-Xe hyperpolarizer [18,19], which operates by the principle of spin exchange optical pumping [20–22]. The flow polarizer produces about 1.5 cm^3/min (@1 bar, 20 °C) Xe gas with a polarization fraction of 20%. The polarized Xe gas flows through the sample cell containing about 0.2 cm^3 of a solvent. For sample preparation, 6 mm of liquid ethanol or an ethanol/water (80 vol% ethanol) mixture was filled into the tip of the transportable sample tube (7 mm inner diameter). The different solvents were first deoxygenated and then frozen at 77 K in a liquid nitrogen bath. A layer of hyperpolarized Xe ice with a thickness of about 1 mm was accumulated over a time period of 6 min onto the surface of the frozen solvent. To maintain the Xe polarization in the sample tube, a field of 1000 G was applied using a permanent magnet. The loss of polarization of the solid Xe at 77 K and 1000 G is negligible due to the long T_1 relaxation rate of 10^{-4} s^{-1} [23]. After the preparation period, the sample tube was closed with two valves, separated from the hyperpolarizer, and finally inserted into a 4.7 T vertical bore Bruker imaging system operating at a Xe resonance frequency of 55 MHz. We used a birdcage resonator with an inner diameter of 20 mm (BRUKER) for all NMR experiments.

A series of two-dimensional FLASH images and one-dimensional spectroscopic images were acquired during the warm-up and melting processes. The corresponding pulse sequences for the spectroscopic and the FLASH images are shown in Figs. 1B and C. The sequence to obtain one-dimensional spectroscopic images consists of an rf-excitation pulse with a small flip angle α followed by a G_z-gradient pulse of 150 μs duration for phase encoding along the z-direction. The bipolar gradient pulse G_x in the x-direction serves to generate a gradient echo. The gradient G_z was increased stepwise from −1 to +1 T/m in 64 steps. The acquisition of the Xe-free induction decay (acquisition time is 20 m) was started after

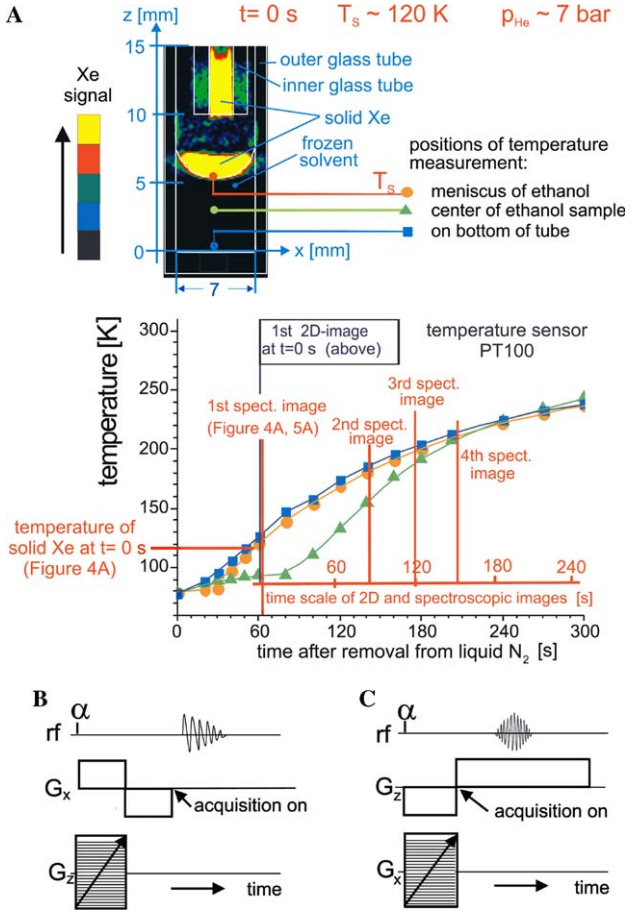

Fig. 1. (A) Two-dimensional x–z FLASH image of hyperpolarized Xe ice frozen on the surface of an ethanol/water ice block. The lower part shows the measured temperature evolution at three positions within the sample. The first 2D FLASH and spectroscopic images ($t = 0$ s) are taken about 60 s after removal of the sample from liquid nitrogen. Note the temperature of Xe ice (117 K) at $t = 60$ s which is determined from the linewidth of the Xe ice spectrum [29]. (B) Pulse scheme for one-dimensional Xe spectroscopic imaging and (C) the FLASH imaging sequence.

switching off the G_x gradient and after a minimum delay time during the gradient fall time. The total time required for a complete 1D image was 2 s and the field of view (fov) was 30 mm along z. Phase transitions and dissolution arising in the process of melting solid Xe on a timescale of several minutes could be measured as a function of time (t) and space (z). To compensate for the losses of Xe magnetization due to T_1-relaxation and rf-pulses, and to optimize the signal-to-noise ratio, the flip angle α was adequately increased from $\alpha = 0.25°$ for the first image to $\alpha = 12°$ for the last image.

The 2D FLASH images were acquired using 64 phase encoding G_x gradient steps along the indirect dimension and by acquiring the gradient echo signal along the direct dimension caused by bipolar G_z gradients. Each 2D FLASH image represents a projection along the direction of the y-axis within the sensitive coil volume since no slice selection was applied and the fov for the images along x and z is 20 mm, respectively. The spatial resolution is about 80 μm in the x-direction and 310 μm in the z-direction.

Fig. 1A top shows a 2D FLASH image of pure hyperpolarized solid Xe frozen on top of the solid ethanol ice block. Note the Xe ice which forms on the surface of the inner glass tube when the flowing hyperpolarized Xe gas freezes at $T = 77$ K. Also indicated in Fig. 1A are the initial conditions, the sample geometry, and the dimensions of the sample. The temperature distribution of both types of sample (100% ethanol, 80/20% ethanol water) inside the tube was measured at a pressure of 1 bar and without frozen Xe in separate runs with a PT 100 sensor inside the sample at three different locations (on the meniscus, in the center of the ethanol, and on the bottom of the tube). The temperatures are independent of the type of sample (pure ethanol, 80/20 vol% ethanol/water) due to the small amount of sample material. The evolution of temperature during the initially frozen sample depends mainly on the heat capacity of the sample tube. Therefore, these measurements give a good estimation of temperature during the NMR experiments. The results of these temperature measurements are shown on the bottom of Fig. 1A. The ^{4}He pressure inside the sample tube during the NMR experiments was 7 bar. At $t = 0$ s (60 s after removal of the sample from the liquid N_2), we measured the first 2D FLASH image ($T \sim 120$ K). Note that the difference in temperature between the meniscus and the bottom is less than 5 K and that the maximum difference is 45 K between the center of the solid ethanol and the bottom of the tube (80 s after removal of the sample from liquid N_2). For $t > 200$ s, the temperature differences in the whole sample are smaller than 5 K.

3. Results and discussion

Our main interest was the investigation of the incorporation and dissolution mechanism of Xe atoms into the frozen solvent matrix during the warm-up period. The two series of FLASH images in Fig. 2 show the different behaviors of hyperpolarized solid Xe migrating into the frozen pure ethanol solid (Fig. 2 top) and 80 vol% ethanol/water ice (bottom). For each image in Fig. 2, the corresponding temperature T_s is denoted, measured on the surface of the frozen solvent. Let us start with the images of pure ethanol (Fig. 2 top). At

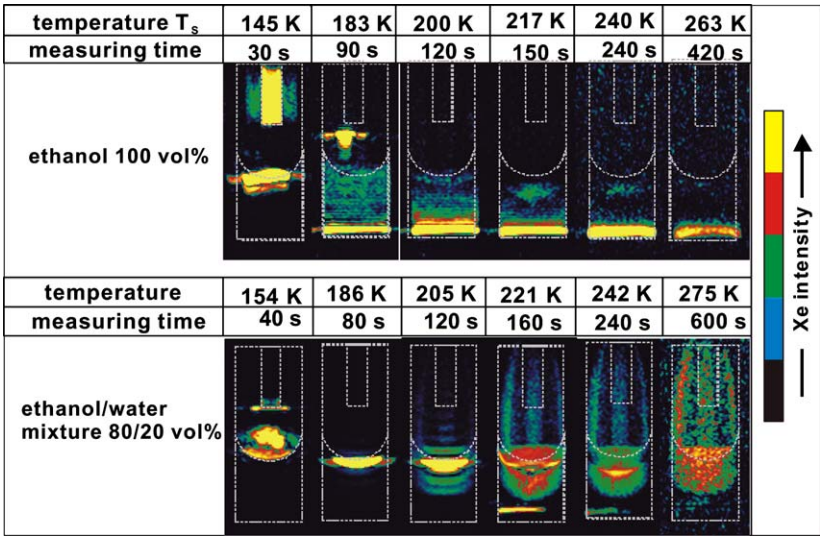

Fig. 2. (Top) Series of two-dimensional FLASH images of hyperpolarized Xe ice, which is melting, migrating, and dissolving into the supercooled ethanol phase. The dotted lines indicate the position of the inner and outer glass tube and the shape of the meniscus. After 120 s, all the Xe polarization is concentrated on the bottom of the outer tube. (Bottom) Corresponding FLASH images for the case of 80 vol% ethanol/water ice. After 600 s, nearly all the Xe polarization is in the gas phase.

$t = 30$ s ($T_s \sim 145$ K) the solid Xe (melting point 161.3 K) starts to sink slowly as a whole block through the ethanol although the melting point of pure ethanol, $T_m^{eth} = 159$ K, is much higher. This can be explained by the phase diagram of ethanol, which shows a supercooled liquid state at temperatures between $97\text{ K} < T < 159\text{ K}$ [24] in the case of fast cooling. At $t = 90$ s ($T_s \sim 183$ K) the solid Xe of the inner tube has melted and forms a liquid droplet at the end of the inner tube. This is consistent with the fact that solid Xe melts at $T_m = 161.3$ K and liquid Xe starts to boil at $T_b = 208$ K at 7 bar. Note the thin layer of Xe with ~1 mm thickness on the bottom of the tube. Some hyperpolarized solid or liquid Xe has moved down from the top of the meniscus through the supercooled ethanol because the Xe (solid, liquid) has a much higher density compared to ethanol. Note that the FLASH images do not provide any information about the physical state and the composition of this thin layer. This will be clarified later by means of spectroscopic imaging. At $t = 120$ s ($T \sim 200$ K) the liquid Xe droplet has fallen through the liquid ethanol and is joining with the Xe layer on the bottom. This layer with a high density of Xe atoms still exists at times $t > 120$ s (Fig. 2 top) and nearly no polarized Xe gas is observable above the liquid although the actual temperature inside the ethanol is much higher than the boiling point of Xe (208 K). A few remarks should be made about the influence of the chemical shifts (solid Xe ~300 ppm, liquid ~250 ppm, and gas = 0 ppm) of different Xe phases onto the images. The dotted lines (meniscus, inner and outer glass tube) are determined by the images of solid Xe (Fig. 1A and Fig. 2 at $t = 30$ s, 40 s). Because the frequency encoding direction was chosen to be the z-direction, the images of the Xe liquid phase are displaced by about 0.8 mm and the gas phase by about 5 mm along the negative z-direction, relative to the image of the solid Xe as a result of their chemical shift differences. For example at $t = 90$ s, the liquid droplet is positioned about 1 mm below the end of the inner tube and the image of the gas phase is shifted almost entirely into the liquid ethanol phase. This overlap of different coexisting Xe phases complicates a quantitative evaluation. Note the sideways displacement of the liquid droplet to the left side of the outer surface of the inlet glass tube. This is a real effect due to imperfect shape and alignment of the inlet, and surface tension of the liquid.

The images on the bottom in Fig. 2 show the melting process of hyperpolarized Xe frozen on top of a solid ethanol/water mixture. The water increases the melting point of the solid ethanol/water to 210 K. This is close to the boiling point of liquid Xe at 7 bar. Consequently, the ethanol/water sample is still in the solid phase when Xe reaches the boiling point. Between $t = 40$ s and $t = 120$ s most of the solid/liquid Xe remains on top of the solid solvent. Note the displacement of the liquid or dissolved Xe phase by $\Delta z = -0.8$ mm from the surface due to the chemical shift difference between the Xe ice and liquid phase. At $t = 160$ s ($T_s = 221$ K) a large fraction of liquid Xe has transformed into the gas phase. The gas image clearly shows the meniscus and the inner tube (two dark vertical stripes) shifted by $\Delta z = -5$ mm. In addition, two thin layers of liquid or dissolved Xe are visible on the surface and close to the bottom of the ethanol/water volume. The explanation for this is that some liquid Xe migrates through pores and/or cracks, which have formed in the solid ethanol/water block. Evidence for the existence of pores will be given later in the spectroscopic images, where the chemical shift information specifies the phase of the Xe. At $t = 600$ s nearly all the remaining Xe polarization is in the gas phase.

To obtain a reference for the interpretation of the spectroscopic images, we measured NMR spectra of thermally polarized Xe in pure ethanol at different temperatures and pressures. At each temperature a Xe spectrum was measured by averaging over 32 scans (50°-pulses, 10 s repetition time) as presented in Fig. 3A for $p = 16$ bar. The zero point of the Xe chemical shift (Xe gas peak at zero pressure) is set 9.2 ppm upfield with respect to the gas peak at 16 bar and 295 K [8]. Note that the linewidth of the dissolved Xe peak is narrow (1–2 ppm) for all temperatures. This means that Xe is mobile in the ethanol down to 160 K. Below 160 K the Xe dissolved in ethanol starts to form solid clusters (see line at 298 ppm in Fig. 3A) leading to a lower Xe density in the Xe/ethanol mixture and therefore to a lower chemical shift of the dissolved Xe line (see lines at 223 ppm). The measured Xe densities are shown in Fig. 3B. For comparison we plot also the density of liquid Xe (triangles) versus T [25]. Fig. 3B shows that large densities of Xe can be dissolved in cold ethanol. From these data the corresponding Ostwald solubility of Xe in ethanol increases from $O_s = 2.5$ (water $O_s = 0.11$) at 300 K [26] to $O_s > 100$ for $T < 180$ K. Fig. 3C shows the Xe chemical shift versus temperature at 2 bar (filled squares), 7.5 bar (open circles), 16 bar (filled circles), and 33 bar (open squares). The filled triangles represent our measured chemical shifts of liquid Xe, which decrease linearly with increasing temperature. The slope is in good agreement with the results of Brinkmann and Carr [27]. From these data a simplified physical model based on a model of Jameson et al. [28] can be developed, which describes the dependence of the chemical shift δ on the temperature T, the ethanol density [Eth], and on the dissolved Xe density [Xe_{sol}].

$$\delta = -\sigma_0^{\text{Xe–Eth}}(T)\cdot[\text{Eth}](T) - \sigma_1^{\text{Xe–Xe}}(T)\cdot[\text{Xe}_{\text{sol}}](T) \qquad (1)$$

$\sigma_0^{\text{Xe–Eth}} = \gamma_1 + \gamma_2 \cdot \exp(-E_{\text{Xe}}^{\text{Eth}}/kT)$ is the Xe–ethanol interaction with $\gamma_1 = -0.399$ ppm/amagat, $\gamma_2 = -0.00706$ ppm/amagat and with the activation energy $E_{\text{Xe}}^{\text{Eth}} = -29.3$ meV (1 amagat corresponds to 2.69×10^{19} cm^{-3}). The Xe–Xe interaction depends linearly on the

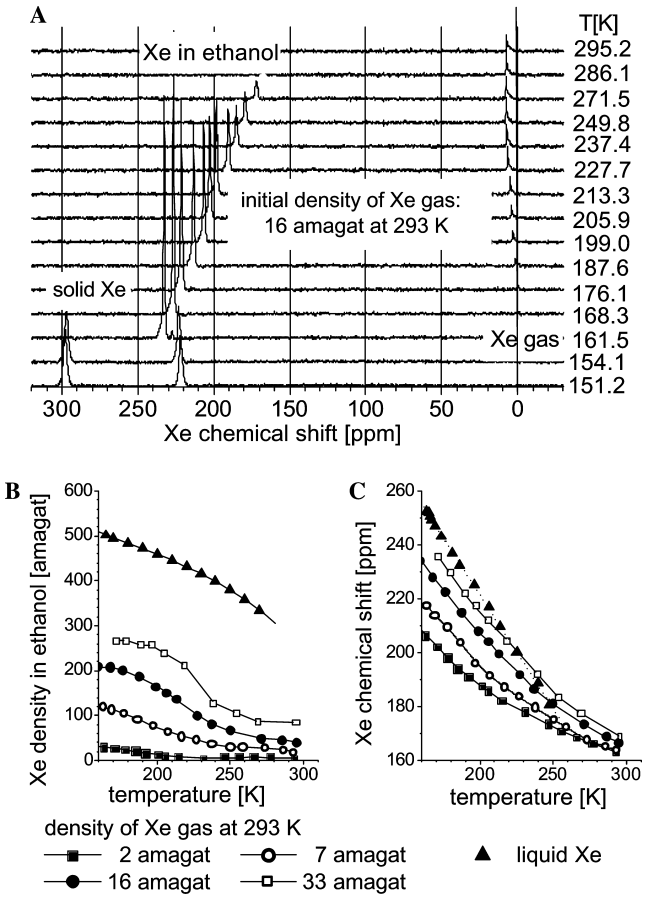

Fig. 3. (A) Thermally polarized Xe NMR spectra versus temperature from a sample tube containing 16 bar of Xe gas and filled with 0.3 cm^3 liquid ethanol. (B) Density of dissolved Xe in ethanol. For comparison the density of liquid Xe (triangles) is shown. (C) Xe chemical shift versus temperature at four initial gas pressures. For comparison the chemical shift of liquid Xe versus temperature is indicated by the triangles. The maximum measured Xe density in ethanol ($T = 165$ K, 33 bar) is about 300 amagat which is about half of the density of liquid Xe (590 amagat). The solid lines in (B) and (C) serve as a guide to the eye.

Xe density over the whole range up to the density of liquid Xe and the coefficient $\sigma_1^{\mathrm{Xe-Xe}}(T)$ depends weakly on temperature and the dominant temperature independent coefficient is $\sigma_1^{\mathrm{Xe-Xe}} = -0.48$ ppm/amagat.

Let us now analyze the spectroscopic images. Figs. 4A–F present a selection of six one-dimensional Xe spectroscopic images in pure ethanol. They show all the coexisting different Xe phases resolved in the spectral, spatial, and time dimension. The horizontal axis in the plots of Fig. 4 represents the spectroscopic dimension of the Xe chemical shift ranging from 0 to 350 ppm. The vertical axis is the amplitude of the spectrum and the third axis gives the z position, where $z = 0$ mm is the bottom of the sample and $z = 6.5$ mm is the lowest point of the ethanol meniscus. Fig. 4A shows the pure Xe ice phase at 300 ppm, which corresponds to the 2D image at $t = 0$ s in Fig. 1A. The intensity in Fig. 4A indicates that most of the solid Xe is frozen on top of the

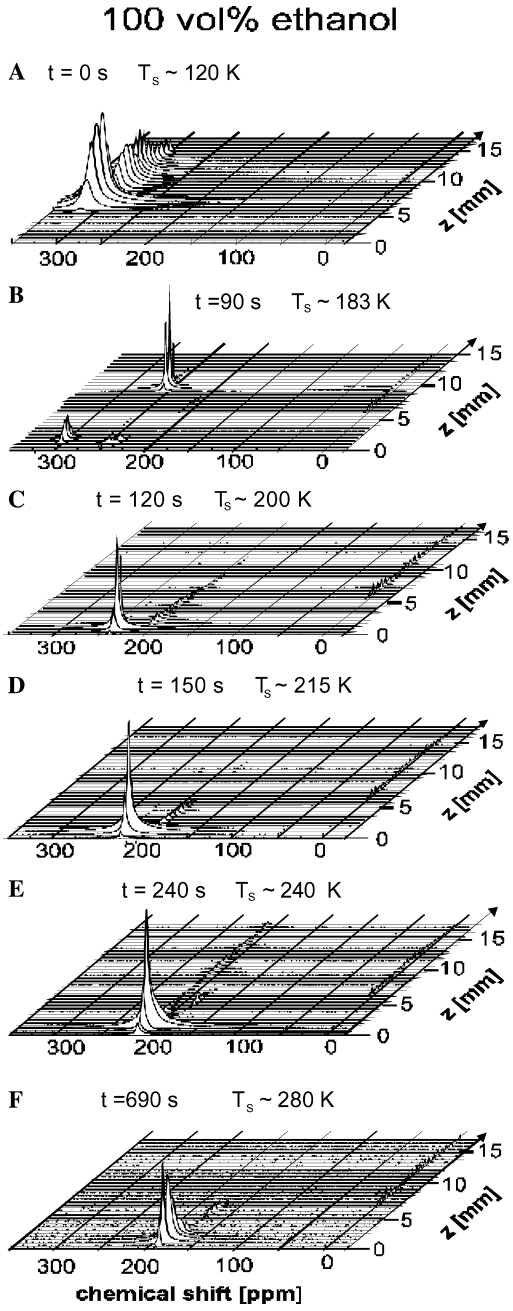

Fig. 4. (A–F) One-dimensional spectroscopic images of hyperpolarized Xe frozen on ethanol ice versus time. The localized spectra give information about all the phase transitions of Xe occurring during the melting and dissolution processes.

meniscus (6–9 mm). The linewidth of the solid Xe varies from 14 ppm (~800 Hz FWHM) at $z = 6.5$ mm to less than 1 ppm (~50 Hz FWHM) at $z = 15$ mm. This can be explained by differences in the temperature within the solid Xe layer at different positions along z. The warmer regions of solid Xe at higher positions z have smaller linewidths because of the increased mobility of the Xe atoms that averages out the static dipole–dipole interaction. Following Yen and Norberg [29], who measured the linewidth of the solid Xe versus temperature, the

temperature of the solid Xe averaged over one slice is estimated to be $T \sim 135\,\mathrm{K}$ at $z = 15\,\mathrm{mm}$ and $T \sim 117\,\mathrm{K}$ at $z = 6\,\mathrm{mm}$. This estimated temperature of 117 K is close to the temperature T_s of 120 K measured with a temperature sensor near the meniscus. The spectroscopic images in Figs. 4B–F show that a thin layer of hyperpolarized Xe has been built up on the bottom of the sample tube. The narrow peaks at 255 ppm in Fig. 4B near $z \sim 10\,\mathrm{mm}$ indicate the liquid Xe droplet, as seen in Fig. 2 ($t = 90\,\mathrm{s}$) at the end of the inner tube. The spectra in the vicinity of $z = 1\,\mathrm{mm}$ show two peaks at 300 and 250 ppm. This means that at $t = 90\,\mathrm{s}$ the thin layer at the bottom is composed of solid Xe particles in coexistence with liquid Xe. Note also in Fig. 5B the trace of Xe spectra at 205 ppm between $6\,\mathrm{mm} < z < 9\,\mathrm{mm}$, which is most likely Xe dissolved in liquid ethanol on the warmer walls of the glass tube. In all the images, only small amounts of Xe gas at 0 ppm exist above the meniscus. At $t = 120\,\mathrm{s}$ (Fig. 4C) all the solid Xe has vanished and the chemical shift of 235 ppm of the thin layer on the bottom of the tube indicates that ethanol molecules start to diffuse into the liquid Xe layer. The chemical shift of this layer drifts from 235 ppm at $t = 120\,\mathrm{s}$ to 195 ppm at $t = 690\,\mathrm{s}$. According to the result of Fig. 3C, this means that the temperature increases and the averaged Xe density within this layer decreases with time. Note that nearly all the Xe polarization is concentrated on the bottom of the sample tube for more than 11 min and this layer exists up to temperatures of 280 K (Fig. 4F). This is far beyond the boiling point of liquid Xe at 208 K at 7 bar. The boiling point of the Xe-ethanol layer increases during the time course of dissolution due to the diffusion of ethanol molecules into the layer, which hinders the evaporation of Xe. The smallest chemical shift of 175 ppm, represented by the small group of lines at $t = 690\,\mathrm{s}$ and between $6\,\mathrm{mm} < z < 8\,\mathrm{mm}$, indicates that the Xe density in this region of the ethanol phase is small.

Nearly all spectra of the Xe layer on the bottom of the tube have very broad linewidths (up to 33 ppm) and have very different and asymmetric lineshapes (Fig. 4). An enhanced view for the different lineshapes is shown for $t = 210\,\mathrm{s}$ in Fig. 6A. The broad and asymmetric lineshapes can be explained by large Xe density gradients (see Fig. 6A) in the radial and in the z-direction, leading to a superposition of narrow lines with different chemical shifts and amplitudes. The extremely broad line width of maximum 33 ppm evidently explains that Xe density variations of about 70 amagat (see Eq. (1)) must exist in the radial and the axial z-direction within our measured sample slice ($\Delta z = 0.5\,\mathrm{mm}$, Δx, $\Delta y = 3.5\,\mathrm{mm}$). Temperature variations of less than 5 K lead to line shifts of smaller than 1.8 ppm and do not explain the observed line broadening.

The spectroscopic images in Figs. 5A–F show the process of the melting, dissolution, and evaporation of hyperpolarized Xe above the frozen ethanol/water ice. In Fig. 5B at $t = 40\,\mathrm{s}$ solid Xe coexists with the liquid and gas phases and a small amount of liquid Xe has penetrated through the whole ethanol/water ice block. At $t = 80\,\mathrm{s}$ (186 K) most of the Xe is in the liquid phase

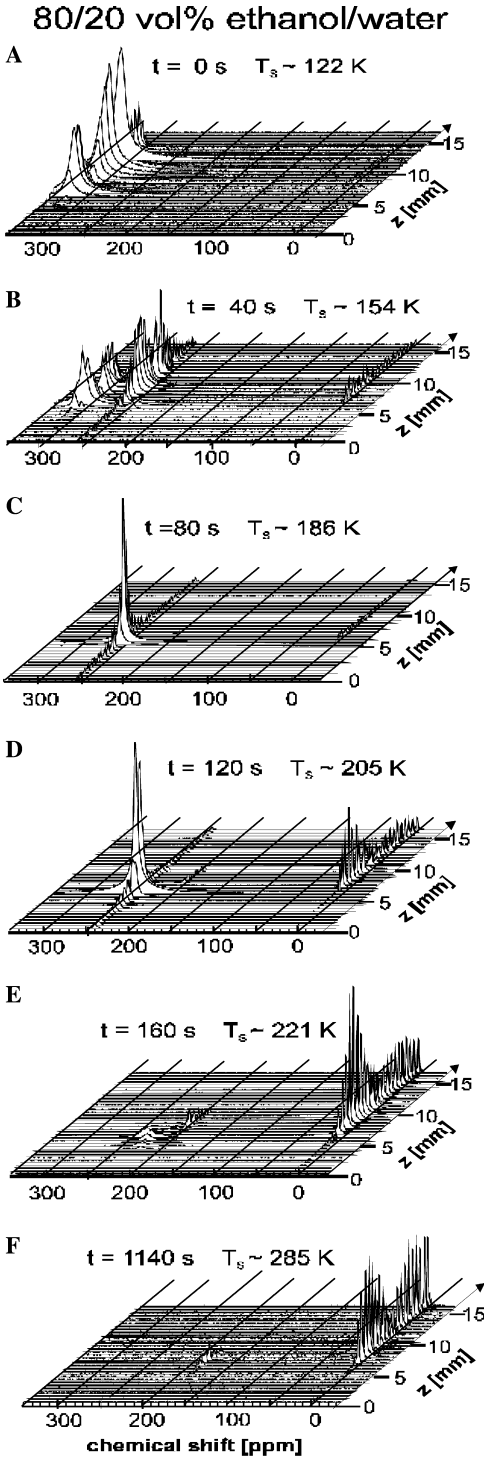

Fig. 5. (A–F) Time series of one-dimensional spectroscopic images of hyperpolarized Xe frozen on 80 vol% ethanol/water ice. These images show different Xe phases (Xe gas, liquid, solid or dissolved phase) well-separated compared to the FLASH-images in Fig. 2.

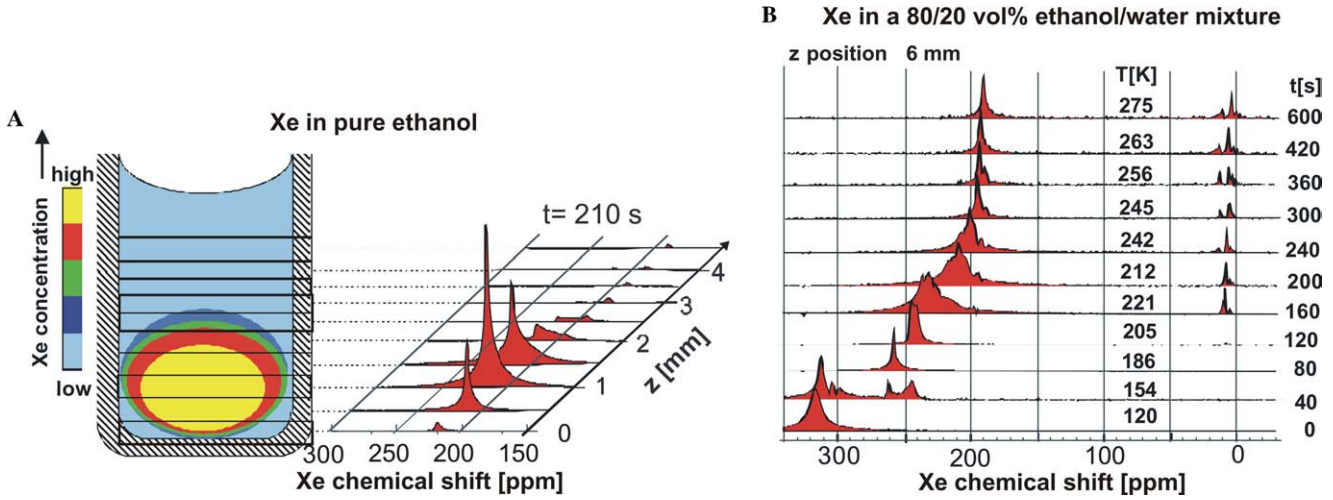

Fig. 6. (A) Enhanced view of the one-dimensional Xe spectroscopic image in pure ethanol for $t = 210$ s. The big changes of the shape and the width of the lines at different positions z can be explained by large variations in the Xe concentration on the bottom of the tube (see Fig. 3B). (B) Time dependence of the Xe spectrum for an 80 vol% ethanol/water mixture measured inside the ice block at $z = 6$ mm. The Xe gas peaks with a chemical shift of a few ppm appearing after $t = 120$ s are associated with closed and open pores filled with Xe gas at different pressures.

(255 ppm chemical shift) and the liquid is concentrated on the surface of the ethanol/water ice block in analogy to Fig. 2 at $t = 80$ s. At $t = 120$ s (Fig. 5D) the measured temperature on the surface $T_s \sim 205$ K is close to the boiling point of liquid Xe (~208 K at 7 bar). Therefore, the liquid Xe has started to evaporate into the gas phase, as indicated by the increased amplitude of the Xe gas spectra above the meniscus. The small group of lines at 200 ppm in the range of the meniscus represents the dissolution of Xe into a liquid ethanol/water layer on the warmer surface of the outer glass tube. At $t = 160$ s (Fig. 5E) most of the hyperpolarized Xe is in the gas phase. The ethanol/water ice block ($T_m = 210$ K) exists several hundred seconds after all the liquid Xe has evaporated. The spectrum below the meniscus ($z <$ 6.5 mm) in Fig. 5E shows a row of Xe gas lines with very small amplitudes and chemical shifts of a few ppm, which originated from the migration of liquid Xe through the pores of the solvent ice matrix and subsequent evaporation. These gas lines inside the melting ethanol/water ice block remain until $t = 600$ s.

The enhanced view in Fig. 6B of the time series of Xe-spectra at the meniscus ($z = 6$ mm) shows a group of gas lines with different chemical shifts for $t > 120$ s. These can be associated by the presence of open and closed pores existing inside the ethanol/water ice block which are filled with Xe gas of different pressures. The broad lines at 220 ppm in Fig. 5E between $3\text{ mm} < z < 6\text{ mm}$ indicate that a fraction of the Xe has dissolved into the liquid ethanol/water phase coexisting with the ice matrix. Again, the large Xe density gradients cause the broad lines with very different lineshapes at different z-positions. After 1140 s (Fig. 5F), the whole ethanol/water ice block has melted and the corresponding spectroscopic image shows that only two lines have survived, Xe gas at $z > 6.5$ mm and Xe dissolved in the liquid meniscus (180 ppm) between $6\text{ mm} < z < 9\text{ mm}$. The fact that no Xe signal can be observed inside the liquid ($z < 6$ mm) except in the vicinity of the meniscus means that all the magnetization of the dissolved Xe has decayed to zero and that the liquid surface is in continuous exchange with the Xe gas reservoir. The large polarization of the frozen Xe ice may be preserved in the liquid alcohol/water mixture by rapidly heating up the sample, which leads to strong convective mixing of Xe into the solvent.

4. Conclusions and outlook

Using the method of time resolved laser-polarized Xe spectroscopic imaging we have demonstrated for the first time how Xe atoms incorporate and dissolve into different frozen solvents. A wealth of different physical phenomena, such as the observation of phase transitions, the position dependent line narrowing of Xe ice, the creation of pores, and the existence of a dense liquid Xe layer in ethanol have been observed. However, the chemical shift of the Xe spectra depends on temperature and on the Xe density and the linewidths on density and temperature gradients, so the spectra under the condition of very high Xe densities in solution have to be interpreted carefully.

The dense liquid Xe/ethanol mixture is promising for the injection into biochemical or biological systems in vitro, where the highest possible density of polarized Xe atoms should be delivered to the target molecules in the aqueous environment. Other applications of Xe spectroscopic imaging, such as the mapping of temperature and gas density versus space and the in situ measurement of chemical reactions in micro-fluid reactors, appear feasible as well.

Acknowledgments

The authors gratefully acknowledge generous support from H. Halling and excellent technical assistance from U. Sieling and G. D'Orsaneo. S. Han acknowledges the generous support from P. Bluemler and H. W. Spiess.

References

[1] M.S. Albert, G.D. Cates, B. Driehuys, W. Happer, B. Saam, C.S. Springer, A. Wishnia, Nature 370 (1994) 199.
[2] S.D. Swanson, M.S. Rosen, B.W. Agranoff, K.P. Coulter, R.C. Welsh, T.E. Chupp, Magn. Reson. Med. 38 (1997) 695.
[3] G. Navon, Y.-Q. Song, T. Rõõm, S. Appelt, R.E. Taylor, A. Pines, Science 271 (1996) 1848.
[4] T. Rõõm, S. Appelt, R. Seydoux, E.L. Hahn, A. Pines, Phys. Rev. B 55 (1997) 11604.
[5] A. Bifone, Y.-Q. Song, R. Seydoux, R.E. Taylor, B.M. Goodson, T. Pietrass, T.F. Budinger, G. Navon, A. Pines, Proc. Natl. Acad. Sci. USA 93 (1996) 12932.
[6] R.J. Fitzgerald, K.L. Sauer, W. Happer, Chem. Phys. Lett. 284 (1998) 87.
[7] T. Pietraß, Magn. Reson. Rev. 17 (2000) 263.
[8] E. Brunner, Concept. Magn. Reson. 11 (1999) 313.
[9] I.L. Moudrakovski, A. Sanchez, C.I. Ratcliffe, J.A. Ripmeester, J. Phys. Chem. B 104 (2000) 7306.
[10] J.P. Butler, R.W. Mair, D. Hoffmann, M.I. Hrovat, R.A. Rogers, G.P. Topulos, R.L. Walsworth, S. Patz, J. Phys.: Condens. Matter 14 (2002) L297.
[11] T. Pietraß, H.C. Gaede, A. Bifone, A. Pines, J.A. Ripmeester, J. Am. Chem. Soc. 117 (1995) 7520.
[12] I.L. Moudrakovski, C.I. Ratcliffe, J.A. Ripmeester, Angew. Chem. Int. Ed. 40 (2001) 3890.
[13] D.W. Davidson, Y.P. Handa, J.A. Ripmeester, J. Phys. Chem. 90 (1986) 6549.
[14] V.J. Storhaug, F. Liebig, C.R. Bowers, J. Phys. Chem. B 106 (2002) 2884.
[15] C.H. Tseng, R.W. Mair, G.P. Wong, D. Williamson, D.G. Gory, R.L. Walsworth, Phys. Rev. E 59 (1999) 1785.
[16] R.W. Mair, C.-H. Tseng, G.P. Wong, D.G. Cory, R.L. Walsworth, Phys. Rev. E 61 (2000) 2741.
[17] I.L. Moudrakovski, S. Lang, C.I. Ratcliffe, B. Simard, G. Santyr, J.A. Ripmeester, J. Magn. Reson. 144 (2000) 372.
[18] S. Appelt, F.W. Häsing, S. Baer-Lang, N.J. Shah, B. Blümich, Chem. Phys. Lett. 348 (2001) 263.
[19] B. Driehuys, G.D. Cates, E. Miron, K. Sauer, D.K. Walter, W. Happer, Appl. Phys. Lett. 69 (1996) 1668.
[20] W. Happer, E. Miron, S. Schaefer, D. Schreiber, W.A. van Wijngaarden, X. Zeng, Phys. Rev. A 29 (1984) 3092.
[21] T.G. Walker, W. Happer, Rev. Mod. Phys. 69 (1997) 629.
[22] S. Appelt, A. Ben-Amar Baranga, C.J. Erickson, M.V. Romalis, A.R. Young, W. Happer, Phys. Rev. A 58 (1998) 1412.
[23] N.N. Kuzma, B. Patton, K. Raman, W. Happer, Phys. Rev. Lett. 88 (2002) 147602.
[24] T. Eguchi, G. Soda, H. Chiara, Mol. Phys. 40 (1980) 681.
[25] W.B. Streett, L.S. Sagan, L.A.K. Staveley, J. Chem. Thermodyn. 5 (1973) 633.
[26] E. Johansson, J. Svensson, S. Månsson, J.S. Petersson, L.E. Olsson, K. Golman, F. Ståhlberg, J. Magn. Reson. 159 (2002) 68.
[27] D. Brinkmann, H.Y. Carr, Phys. Rev. 150 (1966) 174.
[28] C.J. Jameson, A.C. deDios, J. Chem. Phys. 97 (1992) 417.
[29] W.M. Yen, R.E. Norberg, Phys. Rev. 131 (1963) 269.